Light scattering from 2D arrays of monodispersed Ag-nanoparticles separated by tunable nano-gaps: spectral evolution and analytical analysis of plasmonic coupling

Sajal Biring,[1,2] Huai-Hsien Wang,[2,3] Juen-Kai Wang[2,4,*] and Yuh-Lin Wang[2,3,‡]

[1]*Taiwan International Graduate Program, Department of Chemistry, National Tsing-Hua University, Hsinchu, Taiwan*
[2]*Institute of Atomic and Molecular Sciences, Academia Sinica, Taipei, Taiwan,*
[3]*Department of Physics, National Taiwan University, Taipei, Taiwan*
[4] *Center for Condensed Matter Sciences, National Taiwan University, Taipei, Taiwan*
*Corresponding authors: *jkwang@ntu.edu.tw, ‡ylwang@pub.iams.sinica.edu.tw*

Abstract: Two dimensional arrays of monodispersed Ag-nanoparticles separated by different gaps with sub-10 nm precision are fabricated on anodic alumina substrates with self-organized pores. Light scattering spectra from the arrays evolve with the gaps, revealing plasmonic coupling among the nanoparticles, which can be satisfactorily interpreted by analytical formulae derived from generic dipolar approximation. The general formulism lays down a foundation for predicting the *Q* factor of an array of metallic nano-particles and its geometric characteristics.

OCIS codes: (290.5850) Scattering: Particles; (160.4236) Materials: Nanomaterials

References and links

1. M. Faraday, "On the color of colloidal gold," Phil. Trans. R. Soc. London **147,** 145-181 (1857**)**.
2. G. Mie, "Beitrage zur optik truber medien speziel kolloidaler metallosungen," Ann. Phys. **25**, 377-445 (1908**)**.
3. M. Geissler and Y. Xia, "Patterning: Principles and some new developments," Adv. Mater. **16**, 1249-1269 (2004).
4. W. L. Barnes, A. Dereux, and T. W. Ebbesen, "Surface plasmon subwavelength optics," Nature **424,** 824-830 (2003).
5. H. Raether, *Excitation of Plasmons and Interband Transitions by Electrons* (Springer-Verlag, Berlin, 1980), pp. 116.
6. M. Moskovits, "Surface enhanced spectroscopy," Rev. Mod. Phys. **57**, 783-826 (1985).
7. J. C. Hulteen and R. P. Van Duyne, "Nanosphere lithography: A materials general fabrication process for periodic particle array surfaces," J. Vac. Sci. Technol. A **13**, 1553-1558 (1995).
8. H. H. Wang, *et al*., "Highly Raman Enhancing-Substrates Based on Silver nanoparticle Arrays with Tunable Sub-10 nm Gaps," Adv. Mater. **18**, 491-495 (2006).
9. S. Nie and S. R. Emory, "Probing Single Molecules and Single Nanoparticles by Surface-Enhanced Raman Scattering," Science **275**, 1102-1106 (1997).
10. K. H. Su, Q. H. Wei, X. Zhang, J. J. Mock, D. R. Smith, and S. Schultz, "Interparticle coupling effects on plasmon resonances of nanogold particles," Nano Lett. **3**, 1087-1090 (2003).
11. L. Gunnarsson, T. Rindzevicious, J. Prikulis, B. Kasemo, M. Käll, S. Zou, and G. C. Schatz, "Confined Plasmons in Nanofabricated Single Silver Particle Pairs: Experimental Observations of Strong Interparticle Interactions," J. Phys. Chem. B **109**, 1079-1087 (2005).
12. P. K. Jain, W. Huang, and M. A. El-Sayed, "On the universal scaling behavior of the distance decay of plasmon coupling in metal nanoparticle pairs: A Plasmon Ruler Equation," Nano Lett. **7**, 2080-2088 (2007).
13. C. L. Haynes, A. D. McFarland, L. L. Zao, R. P. Von Duyne, G. C. Schatz, L. Gunnarsson, J. Prikulis, B. Kasemo, and M. Käll, "Nanoparticle Optics: The Importance of Radiative Dipole Coupling in Two-Dimensional Nanoparticle Arrays," J. Phys. Chem. B **107**, 7337-7342 (2003).
14. W. Rechberger, A. Hohenau, A. Leitner, J. R. Krenn, B. Lamprecht, and F. R. Aussenegg, "Optical properties of two interacting gold nanoparticles," Opt. Commun. **220**, 137-141 (2003).
15. J. P. Kotmann and O. J. F. Martin, "Plasmon resonant coupling in metallic nanowires," Opt. Express **8**, 655-663 (2001).
16. X. -D. Xiang, *et al*., "A Combinatorial Approach to Materials Discovery," Science **268**, 1738-1740 (1995).

#94020 - $15.00 USD Received 31 Mar 2008; revised 28 Apr 2008; accepted 15 May 2008; published 15 Sep 2008

17. B. N. J. Persson and A. Liebsch, "Optical properties of two-dimensional systems of randomly distributed particles," Phys. Rev. B **28**, 4247-4254 (1983).
18. V. A. Markel, "Coupled Dipole approach to Scattering of Light from a One-Diemnsional Periodic Dipole Structure," J. Mod. Opt. **40**, 2281-2291 (1993).
19. see Appendix.
20. C. F. Bohren and D. R. Huffman, *Absorption and Scattering of Light by Small Particles* (Wiley, New York, 1983), pp. 130.
21. J. D. Jackson, *Classical Electrodynamics*, 3rd ed. (Wiley, New York, 1999), pp. 371.
22. J. D. Jackson, *Classical Electrodynamics*, 3rd ed. (Wiley, New York, 1999), pp. 407.
23. Y. Liu, J. Lin, G. Huang, Y. Guo, and C. Duan, "Simple empirical analytical approximation to the Voigt profile," J. Opt. Soc. Am. B **18**, 666-672 (2001).
24. E. D. Palik, *Handbook of Optical Constants of Solid* (Academic Press, London, 1985), pp. 353.
25. J. J. Olivero and R. L. Longbothum, "Empirical fits to the Voigt linewidth: A brief review" J. Quant. Spectrosc. Radiat. Transfer **17**, 233-236 (1977).
26. B. T. Draine, "The Discrete-Dipole Approxiamtion and its Application to Interstellar graphite Grains," Astrophys. J. **333**, 848-872 (1988).
27. M. J. Collinge and B. T. Draine, "Discrete-dipole approximation with polarizabilities that account for both finite wavelength and target geometry," J. Opt. Soc. Am. A **21**, 2023-2028 (2004).
28. S. Zou and G. C. Schatz, Response to comment on "Silver nanoparticle array structures that produce remarkable narrow plasmon line shapes," J. Chem. Phys. **102**, 122 (2005).
29. B. Khlebtsov, A. Melnikov, B. Zharov, and N. Khlebtsov, "Absorption and scattering of light by a dimmer of metal nanospheres: Comparison of dipole and multipole approaches," Nanotech. **17**, 1437-1445 (2006).
30. C. Voisin, N. D. Fatti, D. Christofilos, and F. Vallee, "Ultrafast Electron Dynamics and Optical Nonlinearities in Metal Nanoparticles," J. Phys. Chem. B, **105**, 2264-2280 (2001).
31. J. D. Jackson, *Classical Electrodynamics*, 3rd ed. (Wiley, New York, 1999), pp. 410.
32. D. W. Thompson, "Optical characterization of porous alumina from vacuum ultraviolet to midinfrared," J. Appl. Phys. **97**, 113511 (2005).

1. Introduction

Since the first study on the color of colloidal gold by Faraday in 1856 [1], the optical properties of an ensemble of metal particles with different sizes, geometries, and spatial arrangements have been a subject of intensive research efforts. With the publication of Mie's scattering theory in 1908 [2], the anomalous optical properties of single gold colloidal particles have been uncovered and are attributed to the collective resonance of its free electrons in response to an impinging electromagnetic wave. Due to the rapid progress of nanofabrication technology [3] in past two decades, the subject took a dramatic renaissance, especially in the search of novel optical properties of large nano-structured systems. This recent development ushered in a new research field called 'plasmonics' [4]. Among many research topics in plasmonics, one of the central themes is to create anomalous optical properties by tailoring the electromagnetic interaction among the nanoparticles. For examples, it is desirable to custom design structures with delocalized electromagnetic resonance characters (surface plasmon polaritons) [5] and to fabricate efficient electromagnetic enhancers for surface-enhanced Raman scattering (SERS) [6]. Especially, uniformly stable SERS measurements have been demonstrated on sculpted metallic surfaces made by nanosphere lithography [7] and metallic nanoparticle arrays embedded in anodic aluminum oxide (AAO) [8]. It is believed that through plasmon coupling 'hot spots' are created in these SERS substrates [9].

The electromagnetic interaction between nanometer-sized particles has been studied experimentally in the case of isolated pairs [10-12] and the arrays [13] of particles fabricated by electron-beam lithography or nanosphere lithography. Through far-field spectroscopic measurements, the observed relationship between scattering spectrum and interparticle spacing was explained by dipole-dipole interaction between the particles [14]. This relationship was also investigated by numerical analysis like discrete dipole approximation [10] and finite-difference time-domain method [15]. However, only qualitative understanding was provided and simple analytical model is still missing, limiting our ability to design arrays of nanoparticles for technological applications. In addition, the experimental studies are limited to large disk-shaped nanoparticles made by electron-beam lithography or complex sculpted structures made by nanosphere lithography and other special deposition techniques [16]. The complex geometry of these nanoparticles renders the interpretation of the spectra difficult. There have been several theoretical efforts in the establishment of simple comprehensive

#94020 - $15.00 USD Received 31 Mar 2008; revised 28 Apr 2008; accepted 15 May 2008; published 15 Sep 2008

models. Persson and Liebsch studied the optical properties of two-dimensional metallic spherical particle arrays and derived an analytical formula for the dependence of the spectral peak on the interparticle spacing [17]. In a study of scattering of light from one dimensional dipole chain, Markel derived an analytical formula for effective polarizability in long-wavelength limit and pointed out the connection between spectral characteristics and electromagnetic interaction [18].

In this study, we investigate inter-particle interaction of arrays of Ag nanorods embedded in AAO nanochannel arrays using light-scattering spectroscopy. Using this system for the study has several advantages. Firstly, well-ordered nanochannels with tunable inter-channel spacings and diameters have been demonstrated with sub-10 nanometer precision [8], enabling the precise fabrication of an array of uniform Ag nanorods with desired size and spatial arrangement. Secondly, with controlled electrodeposition process, Ag nano-rods with smooth geometry can be produced, facilitating simple modeling of the optical properties of these nanorods. Thirdly, these Ag nanorods are surrounded mostly by alumina, which simplifies the effect from the surrounding medium. This is in great contrast to the other systems fabricated by electron-beam lithography and nanosphere lithography. These advantages therefore allow us to derive simple quantitative model to interpret the three spectroscopic characteristics (peak position, width and intensity) acquired from far-field scattering spectra.

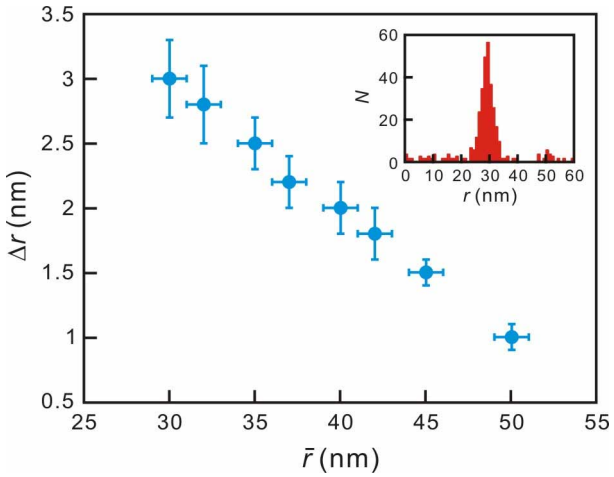

Fig. 1. Variation in interparticle spacing (Δr) *vs*. mean interparticle spacing ($\bar{r}$). Inset shows the histogram of interparticle spacing (r) for a sample with $\bar{r}$ = 30 nm.

2. Sample preparation and measurements

Preparation of silver nanorods inside AAO has been described elsewhere [8]. Briefly, self-organized, hexagonally close-packed AAO nanochannels were fabricated by anodizing an electropolished aluminum foil. The spacing between nanochannels, r, was adjusted by varying the anodization voltage. A fixed diameter of 25 nm was prepared by subsequent etching of the channel walls after the anodization process. Finally, Ag nanorods were grown inside the channels by AC electro-deposition. In the spectroscopy study, the Ag/AAO sample was illuminated in dark-field mode by unpolarized white light from a halogen lamp in an inverted microscope. In dark-field configuration, the sample was illuminated obliquely and the scattered light was collected along the normal to the sample surface. It was then directed to a monochrometer plus charge-coupled device for spectral detection. The smallest mean interparticle spacing, $\bar{r}$, achieved is 30 nm, yielding a mean gap of 5 nm [19]. The corresponding histogram of the interparticle spacing, as given in the inset of Fig. 1, shows a full-width at half-maximum, Δr, of 3 nm. Figure 1 displays Δr as a function of $\bar{r}$ for all the samples prepared for the spectroscopic measurement. A typical scattering spectrum exhibits

#94020 - $15.00 USD Received 31 Mar 2008; revised 28 Apr 2008; accepted 15 May 2008; published 15 Sep 2008

two peaks (not shown), corresponding to the transverse and longitudinal modes [20] of the plasmonic resonance which can be assigned by polarization dependency of these two modes. The rod length of all the samples used in this study was adjusted to be approximately 100 nm such that only the transverse mode is visible in the spectral range of interest.

3. Theory

The Ag nanoparticle arrays in our study can be considered as two-dimensional hexagonal arrays made of Ag prolate spheroids in AAO matrix. In the case of arrays of particles, the local field $\boldsymbol{E}_{loc}(\boldsymbol{r}_i)$ for the particle located at $\boldsymbol{r}_i$ is the sum of the incident field $\boldsymbol{E}_{inc}(\boldsymbol{r}_i)$ and the fields induced by the rest of particles. The effective polarizability of the arrays can be derived accordingly:

$$\alpha_{eff} = \frac{\alpha_T}{1-\alpha_T U}, \tag{1}$$

where $$U = \sum_{j\neq i}\left[\frac{k^2\sin^2\theta_{ij}}{r_{ij}} - \frac{ik\left(3\cos^2\theta_{ij}-1\right)}{r_{ij}^2} + \frac{\left(3\cos^2\theta_{ij}-1\right)}{r_{ij}^3}\right]e^{ikr_{ij}}, \tag{2}$$

α_T is the polarizability of a single prolate spheroid of the transverse mode in an electrostatic field, $k = 2\pi/\lambda$, θ_{ij} is the angle between $\boldsymbol{r}_{ij}$ and $\boldsymbol{E}_{inc}(\boldsymbol{r}_i)$, and $\boldsymbol{r}_{ij} = \boldsymbol{r}_i - \boldsymbol{r}_j$. Considering long-wavelength approximation, Eq. (2) becomes

$$U \approx F\cdot r^{-3} + iB \tag{3}$$

where r is the center-to-center distance between two adjacent particles and F is the lattice sum of the hexagonal particle array. $B = \sum_{j\neq i}\left(3\cos^2\theta_{ij}-1\right)\left[\sin\left(kr_{ij}\right)r_{ij}^{-3} - k\cos\left(kr_{ij}\right)r_{ij}^{-2}\right]$, neglecting the far-field term. It can be shown that the resonance frequency, Ω_T, the corresponding width, Γ, and the peak scattering intensity at Ω_T, $I(\Omega_T)$, are expressed as:

$$\Omega_T^2 = \frac{\omega_p^2\left[1-F\left(S/r\right)^3\right]}{\left(1+C\varepsilon_m\right)+\left(\varepsilon_m-1\right)F\left(S/r\right)^3}, \tag{4}$$

$$\Gamma = \frac{1}{\tau} + \frac{S^3B\omega_p^2}{\left(1+C\varepsilon_m\right)\Omega_T} + \frac{\varepsilon_m-1}{1+C\varepsilon_m}S^3B\Omega_T, \tag{5}$$

and

$$I(\Omega_T) \propto N(r)\Omega_T^4\left|\alpha_{eff}(\Omega_T)\right|^2 = N(r)\left\{\frac{\Omega_T S^3\left[\left(\varepsilon_m-1\right)\Omega_T^2+\omega_p^2\right]}{\Gamma\left(1+C\varepsilon_m\right)}\right\}^2, \tag{6}$$

where ε_m is the dielectric constant of the surrounding medium, $S^3 = R^2h/3L$, $C = (1-L)/L$, R and $2h$ are the radius and the length of the spheroid, respectively, L is the depolarization factor, and $N(r)$ is the surface particle density. In the derivation, Drude model is

#94020 - $15.00 USD Received 31 Mar 2008; revised 28 Apr 2008; accepted 15 May 2008; published 15 Sep 2008

assumed for the dielectric function of Ag with plasma frequency, ω_p, and relaxation time, τ, as parameters. The detailed derivation of Eqs. (4)-(6) is presented in Ref. 19. In the case of arrays of spherical particles in vacuum, the resultant resonance frequency agrees with the derived result by Persson and Liebsch [17] and exhibits a dependence on R/r which was also obtained by many research groups [10-12]. Equation (5) shows that the spectral width is also dependent on the coupling between adjacent particles in the array, which was ignored previously [10-12, 17]. As described above, the coupling by the adjacent dipoles introduces the imaginary term in *U* and therefore extra contributions to the imaginary part of α_{eff}, as shown in Eq. (1). This additional quadrature component in α_{eff} causes effective absorption that reflects the energy flow from a specific dipole to its surrounding dipoles and therefore gives rise to extra broadening in Γ. For narrower interparticle spacings, Ω_T exhibits red shifting and *B* becomes larger, thus leading to an increase in Γ. Finally, Eq. (6) presents the fact that the peak intensity is proportional to the square of the *Q* factor of the system, which is equal to Ω_T/Γ and directly reflects the field strength at the resonance frequency in this plasmonic system [21].

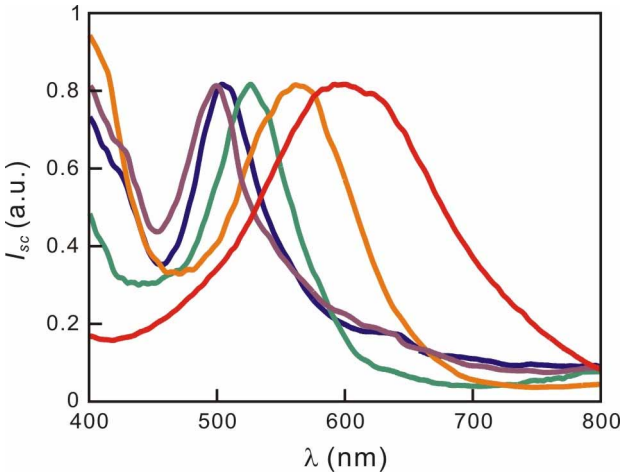

Fig. 2. Normalized scattering spectra from Ag nanoparticle arrays with mean interparticle spacings: 50 nm (violet line), 45 nm (blue line), 40 nm (green line), 35 nm (orange line), and 30 nm (red line).

4. Results and discussion

The physical origin of the observed spectral peak shifting and width broadening induced by plasmonic coupling can be understood using the theoretical framework as described above. There are three spatial regions of interest for the field generated from a single induced-dipole: near, intermediate and far zone [22], which are reflected by the three terms in Eq. (2). The $1/r_{ij}^3$ and $1/r_{ij}$ terms represent the near- and far-zone contributions, respectively, while the $1/r_{ij}^2$ term dominates in the intermediate zone and has a 90° phase shift with respect to the other terms. The far-zone contribution becomes prominent only when r_{ij} is comparable to the wavelength and therefore is insignificant in the discussion of the coupling induced peak shifting and broadening. Because the near-zone term is much larger than the intermediate-zone term under the long-wave approximation, it dominates the real part of *U* in the spatial range of this study, and acts as the single source in the coupling-induced peak shifting. In contrast, both the near- and intermediate-zone terms contribute to the spectral width broadening [18]. Since the broadening is caused by the collective energy transfer between dipoles of different

#94020 - $15.00 USD Received 31 Mar 2008; revised 28 Apr 2008; accepted 15 May 2008; published 15 Sep 2008

separations in the intermediate zone, this effect could not have been revealed by the studies of isolated dipole pairs reported previously [10-12]. Such theoretical understanding allows us to conclude that the spectral peak shifting and width broadening are measures of the plasmonic coupling within the near and intermediate zones.

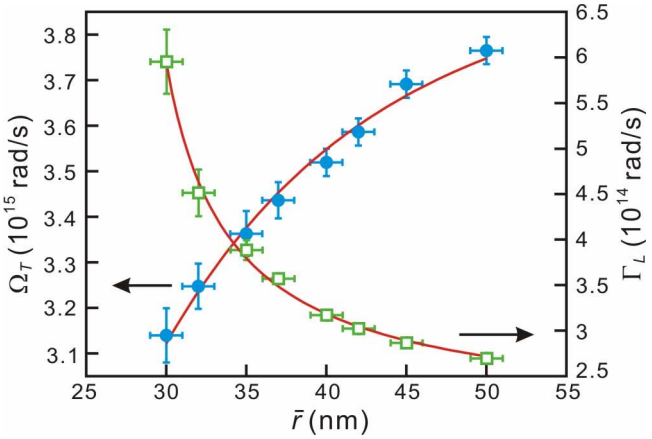

Fig. 3. Transverse-mode resonance peak (Ω_T) and Lorentzian width (Γ_L) *vs.* mean interparticle spacing ($\bar{r}$). Red solid lines are theoretical fittings.

The theoretical derivation above paves a way to analyze scattering spectra of Ag nanorod arrays with different interparticle spacings. The normalized scattering spectra of the five samples with $\bar{r}$ = 30, 35, 40, 45 and 50 nm are shown in Fig. 2. Clearly, the transverse mode is red-shifted and broadened as $\bar{r}$ decreases. This is consistent with previous experimental findings [10-12]. The scattering spectra were fitted with Voigt profile [23] in frequency domain to extract the spectral peak Ω_T and width Γ_V. The dependence of Ω_T on $\bar{r}$ is shown in Fig. 3 and was fitted with Eq. (4). The ω_p obtained from the fitting of Ω_T, as shown in the third column of Table 1, agrees well with that extracted from fitting the optical constant of Ag to the Drude model [24] (in the second column of Table 1).

The spectral peak-shift analysis provides a foundation for subsequent analysis of the line-width broadening. In particular, the dependence of the spectral peak shifting on the interparticle spacing provides a means to incorporate the influence of the variation in the interparticle spacing, presented in Fig. 1, in the analysis of the spectral width broadening data. This bears the resemblance with the inhomogeneous contribution in atomic and molecular spectroscopy. According to Eq. (4), the dependence of the variation in Ω_T, $\Delta\Omega_T$, on the variation in r, Δr, can be derived [19]. This formula was used to calculate the inhomogeneous contribution, which has a Gaussian distribution, to the observed spectral width based on the result in Fig. 1 and the extracted parameters from the spectral peak-shift analysis. On the basis of the relationship between the extracted Voigt width, Γ_V, and $\bar{r}$ [19], the Lorentzian width, Γ_L, was then obtained according to the empirical relation among the Voigt, Gaussian and Lorentzian width [25]. The dependence of the resultant Lorentzian width on $\bar{r}$ is displayed in Fig. 3. Γ_L was then fitted with Eq. (5) to obtain the parameters listed in the fourth column of Table 1. Similar to the spectral peak-shifting analysis, both ω_p and τ obtained from the fitting are in good agreement with that extracted from fitting the optical constant of Ag to the Drude model.

#94020 - $15.00 USD Received 31 Mar 2008; revised 28 Apr 2008; accepted 15 May 2008; published 15 Sep 2008

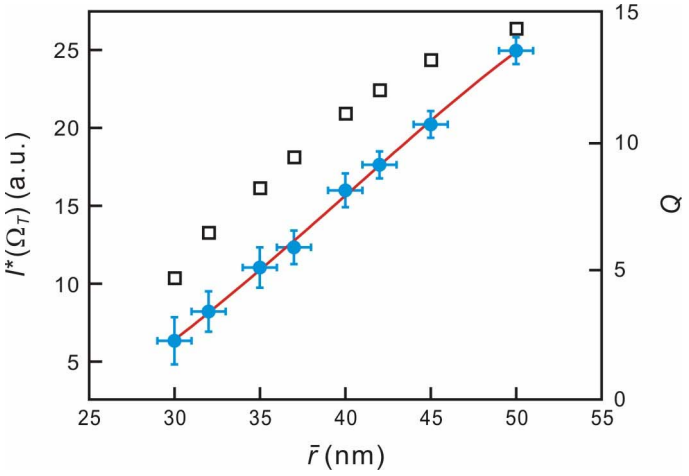

Fig. 4. Scattering intensity at the peak of transverse-mode resonance, $I^*(\Omega_T)$, (filled circles) and Q factor (open squares) *vs*. mean interparticle spacing ($\bar{r}$). Red solid line is a theoretical fitting.

In addition to the spectral peak shifting and width broadening, the scattering intensity also depends on the interparticle spacing, as revealed in Eq. (6). Figure 4 shows the measured average scattering intensity at Ω_T per nanorod, $I^*(\Omega_T)$, as a function of $\bar{r}$, as well as the fitting of Eq. (6) to the data. Again, both ω_p and τ obtained from the fitting, as listed in the fifth column of Table 1, are in agreement with the ones derived from the spectral peak shifting and line-width broadening data. As shown in Eq. (6), $I^*(\Omega_T)$ is proportional to $(\Omega_T/\Gamma)^2$ and therefore to Q^2. Because the transverse mode exhibits red shifting and its line width shows broadening as $\bar{r}$ decreases, $I^*(\Omega_T)$ is expected to decreases monotonically with the decrease in $\bar{r}$, which is consistent with the experimental data shown in Fig. 4. It indicates that the electric field energy stored in the system dissipates faster for smaller interparticle spacings. This $\bar{r}$-dependent energy dissipation behavior can be attributed to the fact that the coupling between dipoles facilitates the energy flow between them, increasing energy loss channels due to electron-phonon scattering, inherent in τ. In addition, as pointed out previously, the Q factor reflects the effective electric field enhancement factor of the system at the resonance frequency. For the applications of using these nanorod arrays in surface-enhanced Raman scattering (SERS) [8], the dependence of Q on $\bar{r}$ provides direct indication how the electromagnetic enhancement factor varies with the interparticle spacing. Since the resonance frequency is varied with the interparticle spacing simultaneously, the actual enhancement factor also depends on the laser wavelength used in Raman scattering. The comprehensive model developed here can thus provide a design tool for SERS-substrates based on plasmonic coupling in nanoparticle arrays.

#94020 - $15.00 USD Received 31 Mar 2008; revised 28 Apr 2008; accepted 15 May 2008; published 15 Sep 2008

Table 1. Comparison of the fitted plasma frequency, ω_p, and relaxation time, τ, of the Drude model from the optical constant, ε, of Ag (Ref. 22) and those from the variation of the spectral peak shifting, Ω_T, the spectral width broadening, Γ_L, and the peak intensity, $I(\Omega_T)$, based on Eqs. (4)-(6). The errors represent the fitting error. The analysis of the fitting results is given in Appendix.

	ε	Ω_T	Γ_L	$I(\Omega_T)$
ω_p (10^{15} rad/sec)	11.9±0.01	8.50±0.07	10.6±0.05	12.2±0.06
τ (10^{-15} sec)	6.2±0.13	---	7.1±0.8	5.55±0.08

The experimental results of the spectral peak shifting, the line width broadening and the peak intensity variation have been shown to fit well with the developed model based on dipole coupling approximation, Eqs. (4)-(6). A question then emerges: Why does the simple dipole-coupling model work so well in our case given the concern that other multipolar contributions may also be significant? The answer to the question may first lie on the fact that the size of the nanorods is small enough and the shape is smooth enough that their polarizability can be simply represented under quasi-static approximation. Two corrections have been proposed to remedy the simplified approximation. Draine has first pointed out that the dipole polarizability needs to include a radiative-reaction correction (a k^3 term) to account for energy conservation [26]. Later on, another k^2 correction term was considered by many groups [27, 28]. Considering the dimension of the nanorods and the wavelengths of interest in our case, both correction terms only make ~3% difference from the uncorrected polarizability. Both of the two terms therefore only play an insignificant role in the analysis of the far-field scattering spectra. Furthermore, the insignifant contribution of the radiative-reaction (k^3 term) indicates that the decrease of the Q factor with the decrease in $\overline{r}$ is caused mainly by the ohmic loss due to the electron-phonon scattering instead of the radiative loss. Another issue of concern is, for a gap as small as 5 nm ($\overline{r}$ = 30 nm), whether the dipole approximation is still valid and therefore other multipolar effects should be included in the analysis. In a recent study of two coupled silver nanospheres, Khlebtsov and coworkers compared the difference in the spectral peak shifting between the calculated results with an electrodynamic dipole approximation as well as a more complete electrodynamic multipole solution [29]. Their results indicate that large deviation in the spectral peak shifting only occurs for $\overline{r}/R < 2.5$, which is consistent with our observation. The simple analytical formulae, Eqs. (4)-(6), are therefore valid in the variation range of the interparticle spacing used in this study.

5. Conclusions

In conclusion, the electromagnetic interaction in arrays of Ag nanorods embedded in AAO has been investigated thoroughly by both experimental and theoretical methods. The unique self-organization property of AAO allows the fabrication of arrays with desired sizes, geometry, and precise gaps. Analytical formulae based on simple dipole approximations have been derived to describe the dependence of spectral peak shifting, width broadening, and intensity of the scattering spectra on the interparticle spacing. These formulae offer unprecedented opportunities to unravel several important subtleties of plasmonic coupling. Specifically, the roles of electromagnetic interactions in various zones can be recognized and characterized quantitatively. These formulae also reveal the dependence of the system's Q factor on the interparticle spacing, which is closely related to the electromagnetic field enhancement of an ensemble of nanoparticles via plasmonic coupling. They therefore can be exploited in the area of nanoparticle-enhanced spectroscopy including Raman scattering, infrared absorption, and fluorescence spectroscopy.

#94020 - $15.00 USD Received 31 Mar 2008; revised 28 Apr 2008; accepted 15 May 2008; published 15 Sep 2008

Acknowledgment

Authors thank the financial supports (NSC-96-2120-M-001-002 and 95-3114-P-001-007-MY3) from the National Science Council and Academia Sinica in Taiwan.

#94020 - $15.00 USD Received 31 Mar 2008; revised 28 Apr 2008; accepted 15 May 2008; published 15 Sep 2008

Appendix

A. SEM and TEM images

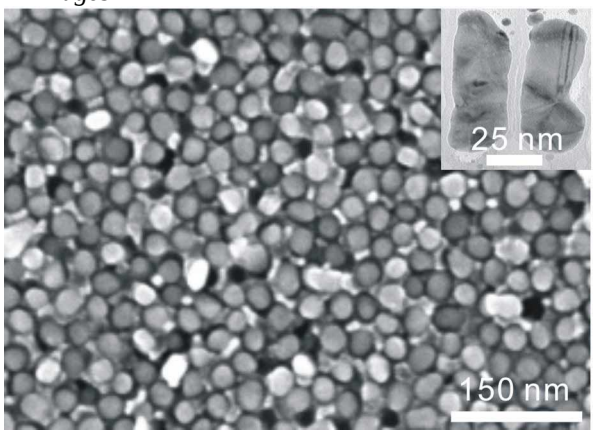

Appendix Fig. 1. Top view scanning electron microscopy image of Ag/AAO substrate with a mean diameter of 25 nm and a mean interparticle spacing of 30 nm. Inset shows the corresponding cross-section transmission electron microscopy image.

B. Derivation of the formula

The Ag nanoparticle arrays in our study can be considered as two-dimensional hexagonal arrays made of Ag prolate spheroids in AAO matrix. The transverse-mode polarizability of a single prolate spheroid along its short axis in an electrostatic field is given by [20]

$$\alpha_T(\omega) = R^2 h \frac{\varepsilon(\omega) - \varepsilon_m}{3\varepsilon_m + 3L\left[\varepsilon(\omega) - \varepsilon_m\right]} \tag{1}$$

where R and $2h$ are the radius and the length of the spheroid. $L = \frac{1}{2} - \frac{1-e^2}{2e^2}\left(-1 + \frac{1}{2e}\ln\frac{1+e}{1-e}\right)$, where $e^2 = 1-(R/h)^2$. ε_m is the dielectric function of the surrounding medium and

$$\varepsilon(\omega) = 1 - \frac{\omega_p^2}{\omega(\omega + i/\tau)} \tag{2}$$

is the dielectric function of the metal particle based on Drude model. ω_p and τ are the plasma frequency and relaxation time, respectively. For silver in the visible wavelength range (400 to 800 nm), ω_p ~ 10^{16} rad/sec and τ ~ 10^{-14} sec [30]. Since $\omega >> 1/\tau$, Eq. (1) can be approximated as

$$\alpha_T(\omega) \approx \frac{\left(\frac{S^3}{1+C\varepsilon_m}\right)\left[(\varepsilon_m - 1)\omega^2 + \omega_p^2\right]}{\frac{\omega_p^2}{1+C\varepsilon_m} - \omega^2 - i\frac{\omega}{\tau}} \tag{3}$$

#94020 - $15.00 USD Received 31 Mar 2008; revised 28 Apr 2008; accepted 15 May 2008; published 15 Sep 2008

where $S^3 = R^2 h/3L$ and $C = (1-L)/L$. It indicates that each particle behaves as a harmonic oscillator (Lorentz model) with a resonance frequency $\omega_p \Big/ \sqrt{(1+C\varepsilon_m)}$ and a damping constant $1/\tau$. In the case of arrays of particles, the local field $\boldsymbol{E}_{loc}(\boldsymbol{r}_i)$ on each particle is the sum of the incident field $\boldsymbol{E}_{inc}(\boldsymbol{r}_i)$ and the fields induced by the rest of particles and can be written as [31]

$$\boldsymbol{E}_{loc}(\boldsymbol{r}_i) = \boldsymbol{E}_{inc}(\boldsymbol{r}_i) + \sum_{j\neq i} \frac{e^{ikr_{ij}}}{r_{ij}^3}\left[k^2 \boldsymbol{r}_{ij} \times (\boldsymbol{r}_{ij} \times \boldsymbol{P}_j) + \frac{1-ikr_{ij}}{r_{ij}^2} \times \left\{ r_{ij}^2 \boldsymbol{P}_j - 3\boldsymbol{r}_{ij}(\boldsymbol{r}_{ij} \cdot \boldsymbol{P}_j) \right\} \right] \quad (4)$$

where $\boldsymbol{r}_{ij}$ is the difference between the position vectors of i-th and j-th particles. Assuming that the local field at each particle is the same, *i.e.* $\boldsymbol{E}_{loc}(\boldsymbol{r}_i) = \boldsymbol{E}_{loc}(\boldsymbol{r}_j)$, and considering $\boldsymbol{P}_j = \alpha_T \boldsymbol{E}_{loc}(\boldsymbol{r}_j)$, the effective polarizability of the arrays can be derived accordingly:

$$\alpha_{eff} = \frac{\alpha_T}{1-\alpha_T U} \quad (5)$$

where $$U = \sum_{j\neq i} \left[\frac{k^2 \sin^2\theta_{ij}}{r_{ij}} - \frac{ik(3\cos^2\theta_{ij}-1)}{r_{ij}^2} + \frac{(3\cos^2\theta_{ij}-1)}{r_{ij}^3} \right] e^{ikr_{ij}} \quad (6)$$

and θ_{ij} is the angle between $\boldsymbol{r}_{ij}$ and $\boldsymbol{E}_{inc}(\boldsymbol{r}_i)$. Notice that *U* depends on the interparticle spacing and the packing configuration of the array. In this study, the Ag nanorod array has a hexagonal packing pattern. With the substitution of Eq. (3), Eq. (5) becomes

$$\alpha_{eff} = \frac{S^3\left[(\varepsilon_m - 1)\omega^2 + \omega_p^2\right]}{\left[(1-S^3A)\omega_p^2 - \left\{(1+C\varepsilon_m) + (\varepsilon_m - 1)S^3A\right\}\omega^2\right] - i\left[(\varepsilon_m - 1)S^3B\omega^2 + (1+C\varepsilon_m)(\omega/\tau) + S^3B\omega_p^2\right]} \quad (7)$$

where A and B are defined as $U = A + iB$. The scattering intensity is then the sum of the scattered radiation from each particle with this effective polarizability. This equation exhibits a quasi-Lorentzian form. The resonance peak in a scattering spectrum emerges as the real part of the denominator vanishes and, therefore, the full-width at half-maximum can be solved accordingly. It also reveals that *A* is responsible for plasmon resonance peak shift, while *B* plays a role in the linewidth broadening and is also a function of the interparticle spacing of the array, *r*. Considering long-wavelength approximation, *i.e.* $\exp(ikr_{ij}) \approx 1$, Eq. (6) becomes

$$U \approx F \cdot r^{-3} + iB \quad (8)$$

where F is the lattice sum of the hexagonal particle array. On the other hand, under the condition of neglecting the far-field term,

#94020 - $15.00 USD Received 31 Mar 2008; revised 28 Apr 2008; accepted 15 May 2008; published 15 Sep 2008

$B = \sum_{j \neq i} \left(3\cos^2\theta_{ij} - 1\right)\left[\sin\left(kr_{ij}\right) r_{ij}^{-3} - k\cos\left(kr_{ij}\right) r_{ij}^{-2}\right]$. The introduced error in the real part of *U* for the wavelength of 550 nm is smaller than 0.5% for the interparticle spacing range considered in this study. The leading term of *B* with a dependence on the interparticle spacing is proportional to $k^5 r_{ij}^2$ which is zero under the long-wavelength approximation. This approximation is therefore not applied the subsequent derivation of *B*. From Eq. (7), we can derive the resonance frequency, Ω_T, the corresponding linewidth, Γ, and the scattering intensity at Ω_T, $I\left(\Omega_T\right)$. According to Eq. (7), Ω_T, corresponding to the maximum value of α_{eff}, can be extracted by solving $\left[\left(1 - S^3 A\right)\omega_p^2 - \left\{\left(1 + C\varepsilon_m\right) + \left(\varepsilon_m - 1\right)S^3 A\right\}\Omega_T^2\right] = 0$ and is given by

$$\Omega_T^2 = \frac{\omega_p^2\left[1 - F\left(S/r\right)^3\right]}{\left(1 + C\varepsilon_m\right) + \left(\varepsilon_m - 1\right)F\left(S/r\right)^3}. \tag{9}$$

Γ can be determined by evaluating the frequency at half of the maximum value of $\left|\alpha_{eff}\right|^2$ and is given by

$$\Gamma = \frac{1}{\tau} + \frac{S^3 B\omega_p^2}{\left(1 + C\varepsilon_m\right)\Omega_T} + \frac{\varepsilon_m - 1}{1 + C\varepsilon_m} S^3 B\Omega_T. \tag{10}$$

Finally, $I\left(\Omega_T\right)$ can be expressed as

$$I\left(\Omega_T\right) \propto N\left(r\right)\Omega_T^4\left|\alpha_{eff}\left(\Omega_T\right)\right|^2 = N\left(r\right)\left\{\frac{\Omega_T S^3\left[\left(\varepsilon_m - 1\right)\Omega_T^2 + \omega_p^2\right]}{\Gamma\left(1 + C\varepsilon_m\right)}\right\}^2, \tag{11}$$

where $N(r)$ is the surface dipole density. To illustrate the physical contents of the spectral peak and width, we can consider the arrays of spherical particles in air. In this case, $\varepsilon_m = 1$, $S = R$ and $C = 2$. Equations (9)-(11) then become

$$\Omega_T = \left(\omega_p / \sqrt{3}\right)\sqrt{1 - F\left(R/r\right)^3}, \tag{12}$$

$$\Gamma = \frac{1}{\tau} + \frac{R^3 B\omega_p^2}{3\Omega_T}, \tag{13}$$

and

$$I\left(\Omega_T\right) \propto N\left(r\right)R^6\omega_p^4\left(\frac{\Omega_T}{\Gamma}\right)^2. \tag{14}$$

In the long-wavelength approximation, *B* becomes zero and Eq. (12) and the resultant line width above are consistent with the derived result by Persson and Liebsch [17].

#94020 - $15.00 USD Received 31 Mar 2008; revised 28 Apr 2008; accepted 15 May 2008; published 15 Sep 2008

C. Voigt linewidth

The dependence of the spectral peak shifting on the interparticle spacing provides a means to incorporate the influence of the variation in the interparticle spacing, presented in Fig. 1, in the analysis of the spectral width broadening data. According to Eq. (9), the dependence of the variation in Ω_T, $\Delta\Omega_T$, on the variation in r, Δr, can be derived as

$$\Delta\Omega_T = \frac{3}{2}\frac{F^2 S^3 \varepsilon_m (C+1)}{\Omega_T r^6 \left[1 + C\varepsilon_m + (\varepsilon_m - 1) F \left(S/r\right)^3\right]^2}\Delta r \tag{15}$$

and were used to calculate the inhomogeneous contribution based on the result in Fig. 1 and the extracted parameters from the spectral peak-shift analysis in the main text. The extracted Voigt width, Γ_V, and $\bar{r}$, is shown in the figure below.

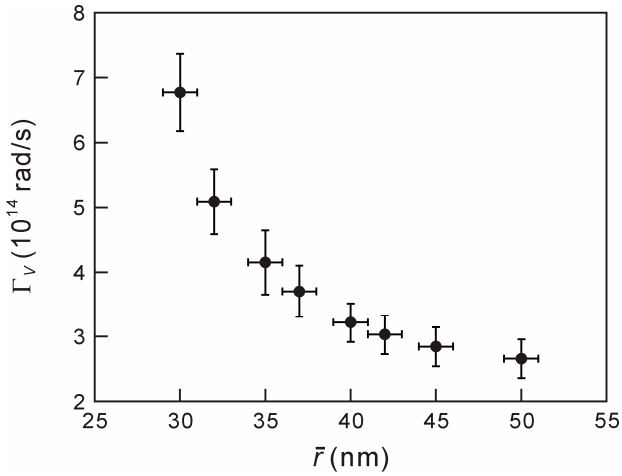

Appendix Fig. 2. Voigt line width (Γ_V) *vs*. mean interparticle spacing ($\bar{r}$).

D. Fitting analysis

The fitted results of the spectral peak shifting *vs*. interparticle spacing with Eq. (9) are shown in Table 1 in the main text. The extracted plasma frequency, ω_p, is just 30% away from the one obtained by fitting the optical constant [24] of Ag to the Drude model within the wavelength range of interest. In the fitting, ε_m was chosen to be the dielectric constant of alumina [32], which is 3 in our case. Since C shows 5% variation for h varied from 25 to 100 nm, C was fixed at 1.2 based on R = 12.5 nm and h = 50 nm. The fitted results of the spectral broadening with Eq. (10) *vs*. interparticle spacing are listed in Table 1 in the main text. The extracted relaxation time, τ, is about 15% higher and ω_p is only 10% less than the one obtained by fitting the optical constants of Ag to the Drude model. Finally, the fitted results of the spectral peak intensity with Eq. (11) *vs*. interparticle spacing yield ω_p and τ which are listed in Table 1 in the main text. Both ω_p and τ match closely with the values obtained from the fitting of the optical constants of Ag with Drude model. In summary, these fitted values comparably agree among themselves and with the values extracted from the dielectric constants of Ag, supporting the fitting process and Eqs. (9)-(11) used in the fitting.

#94020 - $15.00 USD Received 31 Mar 2008; revised 28 Apr 2008; accepted 15 May 2008; published 15 Sep 2008